On the damping deterioration of power systems with CIG-based power plants performing PFR under communication delays

Luna Moreno-Díaz [a,b,*], Juan Manuel Mauricio [b], Álvaro Rodríguez del Nozal [b], Jelena Stojkovic Terzic [c]

[a] Ingelectus Innovative Electrical Solutions, Seville, Spain
[b] Department of Electrical Engineering, Universidad de Sevilla, Seville, Spain
[c] School of Electrical Engineering, University of Belgrade, Belgrade, Serbia

ARTICLE INFO

Keywords:
Primary frequency response
Power park module
Power plant controller
Power oscillation damping
Communication delays
Grid connection code
Small signal analysis

ABSTRACT

The primary frequency response of converter-interfaced generation power plants is a mandatory technical requirement of the grid connection codes. This is the case in Europe, where the grid code EU 2016/631 specifies mandatory frequency sensitive modes for power park modules of medium and high dimension. In this response, the active power output changes as a result of a frequency deviation in order to contribute to the restoration of the nominal frequency. The power plant controller that governs these type of plants is the responsible to perform this task. Plant-level control latency is primarily caused by communication delays, which increase the plant response time, thereby compromising the damping of network oscillation modes in the range of 0.1 to 1.5 Hz. The case presented here shows that in certain situations the primary frequency response, which is crucial for maintaining frequency stability, can seriously affect the oscillation damping of a power system. This can lead to so-called angle instability. Simulations show that PFR provision by PV plants can worsen damping when delays are present, especially with changes in system inertia or line length.

1. Introduction

In modern electrical power systems, the generation mix is undergoing a significant transformation, increasingly combining traditional synchronous machines (SM) with inverter-based resources (IBRs), largely driven by renewable energy integration policies and technological advancements [1]. This shift profoundly impacts system stability. The displacement of synchronous generation by IBRs leads to a critical reduction in system rotational inertia, which inherently compromises frequency stability [2,3]. Furthermore, the high penetration of power electronic devices introduces complex dynamics that affect not only frequency stability but also classical rotor angle and voltage stability, alongside entirely new stability issues related to converter-grid interactions, such as wideband electromagnetic oscillations [3,4]. While these IBRs present stability challenges, they also possess the capability for very fast active power control, enabling potentially faster Primary Frequency Response (PFR) compared to conventional generators [5], creating new challenges and opportunities. Historically, IBRs were not mandated to contribute to frequency regulation, as their grid penetration levels were considered insignificant [6]. However, as the proportion of renewable generation has substantially increased, addressing the associated stability concerns reviewed in [2,3] became mandatory. Consequently, Transmission System Operators (TSOs) worldwide have updated their Grid Connection Codes (GCCs) to introduce PFR requirements for Power Park Modules (PPMs) [7–12]. Generally, PPMs of all sizes must provide active power response during over-frequency events, while medium and large PPMs (often designated Type C and D) are required to deliver PFR for both over- and under-frequency deviations. Focusing on dynamic performance, GCCs typically demand very rapid PFR activation from PPMs, with control latency (termed *initial delay* or *activation time* in GCCs) specified from milliseconds up to a maximum of 2 s, and settling times ranging from a few seconds to 30 s. In Europe, TSOs often require latency to be minimized, as exemplified by the requirement in Spain for PFR latency below 500 ms in the mainland [13] and below 150 ms in the islands [14]. For larger PPMs comprising multiple generating units, PFR is centrally coordinated by a Power Plant Controller (PPC) [15,16]. Achieving the mandated fast plant-level response time, however, remains an operational challenge, influenced by communication network delays between the PPC and individual units, as well as the computation times of control devices, potentially compromising the required dynamic performance [2,16,17].

* Corresponding author at: Department of Electrical Engineering, Universidad de Sevilla, Seville, Spain.
E-mail address: lmoreno@ingelectus.com (L. Moreno-Díaz).

Available online 27 August 2025

The integration of high levels of IBRs introduces numerous operational and stability challenges into modern power systems [18]. While these encompass a wide range of issues from reduced inertia to complex converter interactions, this work focuses specifically on the impact of communication and control delays associated with IBRs providing PFR. Such delays are significant as they can adversely affect system dynamics, potentially worsening the damping of low-frequency electromechanical oscillations [19]. Recent research increasingly examines the dynamic performance and stability implications of IBRs providing PFR, driven by the significant challenges arising in low-inertia power systems, as comprehensively reviewed in [20]. This body of work includes investigations into control interactions and power oscillations across various renewable penetration levels [21], comparisons of different modelling approaches and PFR dynamics in frequency stability assessments [22], and explorations of frequency limits under rapid PFR settling times [23]. While these studies provide valuable insights, a common simplification in many analyses [21–23] is the representation of the PFR activation speed, often focusing on the ramp rate or settling time rather than explicitly modelling the initial control latency (the time lag before the response initiates). This latency, resulting from measurement, communication, and computation delays highlighted as a concern in low-inertia environments [20], is critical as it can introduce phase shifts detrimental to the damping of system oscillations. A notable study addressing these delays is [17], which performs a time-domain analysis of PFR performance considering different communication delay components and their effect on frequency deviations. Yet, while [17] evaluates the impact of delays on frequency nadir, it does not provide a quantitative assessment of how PFR latency specifically affects the damping of low-frequency electromechanical oscillations or identify the critical modes most sensitive to these delays. Consequently, a gap remains in thoroughly analysing and quantifying the influence of realistic PFR activation delays from IBRs on power system oscillatory stability. Based on that, the primary contributions of this paper are:

- To present a discrete-time modelling framework specifically tailored for small-signal stability analysis of power systems with IBRs providing PFR, explicitly incorporating variable control activation latency.
- To quantify the detrimental impact of IBR PFR activation latency on the damping of low-frequency electromechanical oscillations.
- To Identify critical PFR latency thresholds and the specific oscillation modes most adversely affected by delays.

The rest of the paper is organized as follows. Section 2 presents the description of the problem together with the methodology defined to model and discretize the system. In Section 3 some simulation results are presented in which the effect of the communication delays in the oscillatory modes of the system are evaluated. Finally, in Section 4 some conclusions and further work lines are drawn.

2. Methodology for system modelling

This paper analyses the effect of the provision of PFR by a PPM on the different oscillation modes of a power system. For this purpose, different values of the control latency are considered as well as different typologies for modelling these delays. In order to perform this analysis, a methodology with the following steps is used:

- First, a Phasor-domain Differential Algebraic Equation (DAE) model of the power system is built.
- After steady-state computation of the previous DAE system, a Continuous Linear Dynamic Model (CLDM) is obtained.
- Next, a zero order hold discretization is applied to the CLDM in order to obtain a Discrete Linear System Model (DLSM) representation of the power system.
- After that, a dynamic extension is performed over the DLSM in order to consider the PFR loop and the communication delays.
- Finally, a small signal analysis is carried out on the extended model by computing damping coefficients.

In the following, the different steps detailed above are discussed. In particular, first the DAE model of the power system is presented, followed by its discretization. Subsequently, two different alternatives for the modelling of the plant response delays are introduced and integrated in the discrete definition of the system. Finally, the control loop is closed and the method of quantifying the existing oscillation modes is defined.

2.1. Differential algebraic equations model

The considered power system is modelled with a detailed dynamic phasor system of DAE following the [24] approach.

$$\begin{aligned}\dot{\mathbf{x}} &= \mathbf{f}(\mathbf{x},\mathbf{y},\mathbf{u}),\\ \mathbf{0} &= \mathbf{g}(\mathbf{x},\mathbf{y},\mathbf{u}),\\ \mathbf{z} &= \mathbf{h}(\mathbf{x},\mathbf{y},\mathbf{u}),\end{aligned} \tag{1}$$

where $\mathbf{x}$ and $\mathbf{y}$ are, respectively, the dynamic and algebraic states. The inputs are included in the $\mathbf{u}$ vector. Therefore, the system is defined with a set of differential equations $\mathbf{f}$ and algebraic equations $\mathbf{g}$. Additional equations $\mathbf{h}$ are considered to obtain some relevant outputs included in vector $\mathbf{z}$.

Once the equations describing the power system have been defined in the form of (1), the system is linearized as:

$$\begin{aligned}\Delta\dot{\mathbf{x}} &= \mathbf{F}_{\mathbf{x}}^{\mathbf{0}}\Delta\mathbf{x} + \mathbf{F}_{\mathbf{y}}^{\mathbf{0}}\Delta\mathbf{y} + \mathbf{F}_{\mathbf{u}}^{\mathbf{0}}\Delta\mathbf{u},\\ \mathbf{0} &= \mathbf{G}_{\mathbf{x}}^{\mathbf{0}}\Delta\mathbf{x} + \mathbf{G}_{\mathbf{y}}^{\mathbf{0}}\Delta\mathbf{y} + \mathbf{G}_{\mathbf{u}}^{\mathbf{0}}\Delta\mathbf{u},\\ \Delta\mathbf{z} &= \mathbf{H}_{\mathbf{x}}^{\mathbf{0}}\Delta\mathbf{x} + \mathbf{H}_{\mathbf{y}}^{\mathbf{0}}\Delta\mathbf{y} + \mathbf{H}_{\mathbf{u}}^{\mathbf{0}}\Delta\mathbf{u}.\end{aligned} \tag{2}$$

Next, considering $det\left(\mathbf{G}_{\mathbf{y}}^{\mathbf{0}}\right) \neq \mathbf{0}$, the algebraic states $\Delta\mathbf{y}$ can be explicitly calculated as:

$$\Delta\mathbf{y} = -\left(\mathbf{G}_{\mathbf{y}}^{\mathbf{0}}\right)^{-1}\mathbf{G}_{\mathbf{x}}^{\mathbf{0}}\Delta\mathbf{x} - \left(\mathbf{G}_{\mathbf{y}}^{\mathbf{0}}\right)^{-1}\mathbf{G}_{\mathbf{u}}^{\mathbf{0}}\Delta\mathbf{u}, \tag{3}$$

and, therefore, obtaining a state space representation of the system in which the derivatives of the dynamic states are obtained as a function of these states, the system inputs and the system parameters:

$$\Delta\dot{\mathbf{x}} = \mathbf{A}\Delta\mathbf{x} + \mathbf{B}\Delta\mathbf{u}, \tag{4}$$

$$\Delta\mathbf{z} = \mathbf{C}\Delta\mathbf{x} + \mathbf{D}\Delta\mathbf{u}, \tag{5}$$

with

$$\mathbf{A} = \mathbf{F}_{\mathbf{x}}^{\mathbf{0}} - \mathbf{F}_{\mathbf{y}}^{\mathbf{0}}\left(\mathbf{G}_{\mathbf{y}}^{\mathbf{0}}\right)^{-1}\mathbf{G}_{\mathbf{x}}^{\mathbf{0}}, \tag{6}$$

$$\mathbf{B} = \mathbf{F}_{\mathbf{u}}^{\mathbf{0}} - \mathbf{F}_{\mathbf{u}}^{\mathbf{0}}\left(\mathbf{G}_{\mathbf{y}}^{\mathbf{0}}\right)^{-1}\mathbf{G}_{\mathbf{u}}^{\mathbf{0}}, \tag{7}$$

$$\mathbf{C} = \mathbf{H}_{\mathbf{x}}^{\mathbf{0}} - \mathbf{H}_{\mathbf{y}}^{\mathbf{0}}\left(\mathbf{G}_{\mathbf{y}}^{\mathbf{0}}\right)^{-1}\mathbf{G}_{\mathbf{x}}^{\mathbf{0}}, \tag{8}$$

$$\mathbf{D} = \mathbf{H}_{\mathbf{u}}^{\mathbf{0}} - \mathbf{H}_{\mathbf{y}}^{\mathbf{0}}\left(\mathbf{G}_{\mathbf{y}}^{\mathbf{0}}\right)^{-1}\mathbf{G}_{\mathbf{u}}^{\mathbf{0}}. \tag{9}$$

2.2. System discretization

Although the modelled power system is continuous in nature, the control devices operate at discrete times. In addition, the communication delays between the PPC and the IBR can also be represented more accurately in this domain, as they are pure delays. Therefore, a zero order hold discretization is applied to system (4)–(5) giving the following system:

$$\Delta\dot{\mathbf{x}}_d = \mathbf{A}_d\Delta\mathbf{x}_d + \mathbf{B}_d\Delta\mathbf{u}_d, \tag{10}$$

$$\Delta\mathbf{z}_d = \mathbf{C}_d\Delta\mathbf{x}_d + \mathbf{D}_d\Delta\mathbf{u}_d, \tag{11}$$

where subindex d denotes the discrete-time version of (4)–(5).

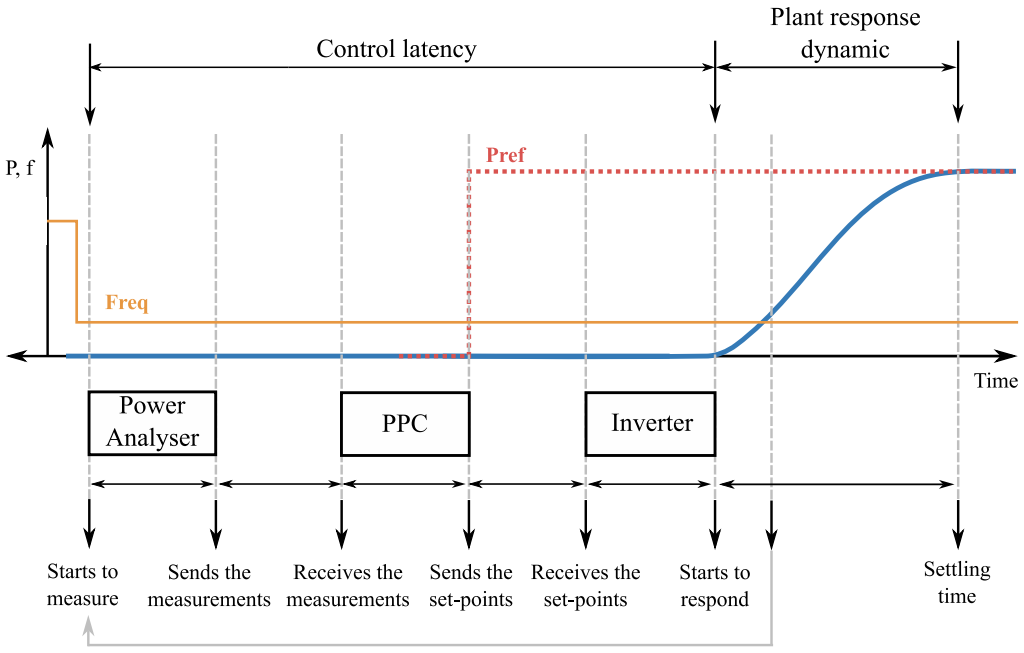

Fig. 1. Response time diagram of a standard PV plant.

2.3. Delays modelling

In this work, the delays under consideration take place from the moment the PPC sends a set-point to the moment a power change is observed at the POI. This time period is designated as the *plant-level control latency*. The sequence of key communication and computation delays involved in this process is shown in Fig. 1 [16,17,25,26]. First, the power analyser measures the system state and sends this information to the PPC. The PPC processes the data and determines the appropriate set-point for each inverter in the plant. Once the inverter receives and processes the set-point, it begins to respond by adjusting its output magnitudes. The last delay of the sequence, specifically the time interval between the inverter receiving a set-point and starting to respond, is generally the most significant and uncertain.

The modelling of plant-level control latency and communication delays is explicitly integrated into the system dynamics through a discrete-time system extension. These delays, which represent the latency from the PPC to the IBR, are categorized as either Single-Step Delay (SSD) or Transportation Delay (TD). SSD assumes sequential communication where the PPC waits for the IBR to process the previous instruction before sending the next one, while TD models periodic, unacknowledged transmissions. Both delay types are represented as multiples of the discretization time step τ and incorporated into the state-space model by augmenting the state vector with additional delay states. This results in a discrete-time extended model where delays are embedded within the state-space representation. A closed-loop formulation then applies the PFR control law directly to this augmented model, enabling the analysis of how different delay values affect system stability through small-signal analysis of the eigenvalues of the resulting system matrix.

In SSD delays different latencies imply different references sent by the PPC as depicted in the upper plot of Fig. 2. This communication is common in the case of centralized controllers where the PPC has the same communication with each converter. On the other hand, in TD delays the latency only affects the time it takes for the IBR to receive the signal as it can be noted in the lower plot of Fig. 2. An example of this type of communication can be the case of peer-to-peer communication or long distance communications like in the case of wide area control [27,28].

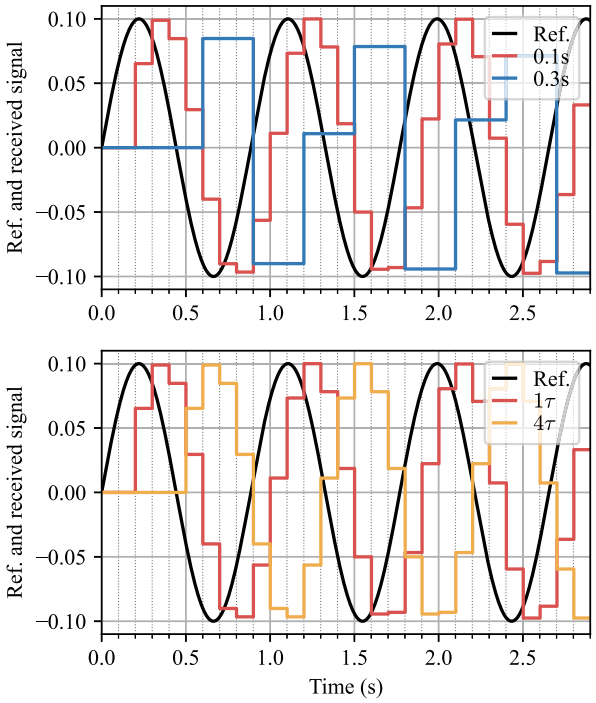

Fig. 2. Carrier signal manged by the PPC and those processed by the IBR.

2.4. Extension for delays modelling

In order to study the dynamic behaviour of the system including the delays in communications, an extension of discrete-time system (10)–(11) is carried out. Prior to that, let us define τ as the time used for the discretization of the system. Thus, the communication latency (for both delay models) can be defined as multiples of τ.

For the SSD model and a delay of 1τ, the state-space extension of the system depicted in red in Fig. 3 is considered, where $\mathbf{I}$ is the identity

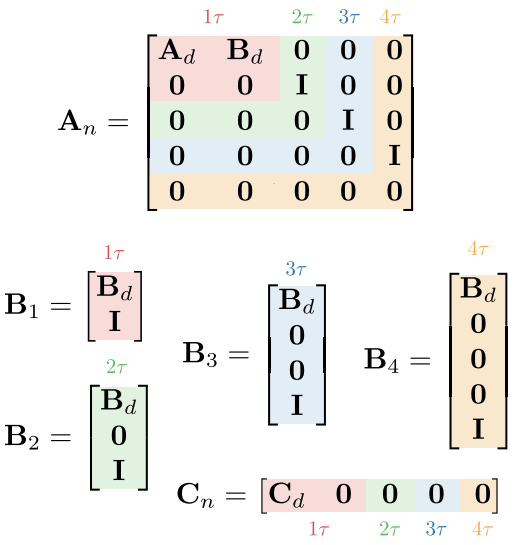

Fig. 3. Linear system matrices for different considered delays.

matrix and $\mathbf{0}$ is a matrix full of zeros of appropriate dimensions. When considering a TD model, the system extension order depends on the steps considered for the delay, being the extension defined in green, blue and yellow for respective 2τ, 3τ and 4τ delays at Fig. 3. The extended system is denoted by the subindex n:

$$\Delta\dot{\mathbf{x}}_n = \mathbf{A}_n\Delta\mathbf{x}_n + \mathbf{B}_n\Delta\mathbf{u}_n, \tag{12}$$

$$\Delta\mathbf{z}_n = \mathbf{C}_n\Delta\mathbf{x}_n + \mathbf{D}_n\Delta\mathbf{u}_n. \tag{13}$$

where the $\Delta\mathbf{x}_n$ vector comprises not only the states from (10) but also the new states modelling the delays involved.

2.5. Closed loop extension

The PFR is implemented using a droop-based frequency controller [7], as shown in Fig. 5. This control law is basically an increase in power that is proportional to, and in the opposite direction to, the frequency deviation:

$$\Delta p_{poi} = -K_f\Delta\omega_{poi}, \tag{14}$$

where K_f is a gain with a value given by the inverse of the so called PFR droop, and ω_{poi} is the frequency of the system at the POI. When working with the DAE model, this frequency can be either a dynamical state or a more complex function of states (i.e. when computing the frequency with a PLL). Generically, it is possible to consider the speed increment as one element of the output vector:

$$\left[\Delta\omega_{poi}\right] = \Delta\mathbf{z}_n = \mathbf{C}_n\Delta\mathbf{x}_n. \tag{15}$$

Therefore, for modelling (12)–(13) in closed loop the input is defined as follows:

$$\Delta\mathbf{u}_n = -K_f\Delta\mathbf{z}_n = -K_f\mathbf{C}_n\mathbf{x}_n. \tag{16}$$

Thus, replacing (16) in (12) it yields:

$$\Delta\dot{\mathbf{x}}_n = \left(\mathbf{A}_n - K_f\mathbf{B}_n\mathbf{C}_n\right)\Delta\mathbf{x}_n = \mathbf{A}_{cl}\Delta\mathbf{x}_n \tag{17}$$

where the matrix $\mathbf{A}_{cl}$ defines the complete dynamics of the discrete-time closed loop system considering the PFR response and communication delays. The complete discrete extended system is represented within the blue box of Fig. 5. The communication delay is incorporated into the control signal path following the PFR output, denoted as Δp. This results in a delayed power reference, designated as Δp_r, which serves as the input to the CLDM.

Table 1
Power system parameters.

Synchronous Machines (Order 4 type):			
Bus **1** S_n = 100 MVA		Bus **4** S_n = 500 MVA	
H = 5.0 s	R_a = 0.01		
X_d = 1.80	X'_d = 0.30	T'_{d0} = 8.0 s	
X_q = 1.70	X'_q = 0.55	T'_{q0} = 0.4 s	
AVR (SEXS type, both machines):			
K_a = 200.0	T_a = 0.10	T_b = 0.10	T_e = 0.10
Governor (TGOV1 type, both machines):			
R = 0.05	T_1 = 1.00	T_2 = 1.00	T_3 = 1.00
Aggregated VSC (coupling inductor type with PQ control):			
X_s = 0.1	R_s = 0.01	S_n = 20 MVA	
Lines and transformers:			
Find parameters at Fig. 4			

2.6. Small signal analysis

A small signal analysis is performed over the extended system defined in (17) by computing eigenvalues of matrix $\mathbf{A}_{cl}$. After that, the discrete system eigenvalues are mapped to the continuous domain applying:

$$\lambda_c = \log\left(\lambda_d\right)/\tau, \tag{18}$$

where λ_c and λ_d are, respectively, the continuous and discrete eigenvalues of the closed-loop system to display the damping loss in a format resembling the ones found in common power system stability textbooks like [29].

The oscillating modes damping are finally computed as:

$$\zeta = \frac{-\Re\left(\lambda_c\right)}{|\lambda_c|}. \tag{19}$$

In the following, the model presented throughout this section will be evaluated under simulation.

3. Results

This section presents the results obtained in simulation. For this purpose, first a test benchmark is presented on which the simulations are performed. This benchmark is modelled according to the methodology proposed in the previous section. Subsequently, an analysis of the dynamic response of the system is carried out when the two types of modelled delays are condemned, analysing the damping of the system.

3.1. Test benchmark

The test system to be analysed is designed to evaluate the effect of a PPM on the oscillation modes of the network to which it is connected (see Fig. 4). In order to define a test system for small signal stability analysis, the Spanish regulation was used as a reference [13]. This standard proposes a two-area benchmark consisting of two synchronous machines interconnected by a transmission line, to which a PPM of large size is connected. Following the same approach, the proposed system has been adapted in terms of size to study the effect of a single type D PPM.

The test benchmark is modelled as a non-linear DAE system (1). Detailed dynamic models of synchronous generators and their controllers have been implemented with the parameters shown in Table 1. The PPM has been modelled as an aggregated power unit considering detailed dynamic models of IBR and PPC with the parameters shown in Table 1. The model has been implemented in continuous time-domain in the power system simulator pydae [30]. More details of the models for each device can be found in the same reference.

A discrete-time PPC controls the PPM at the POI and is in charge of the plant level frequency control. The discrete control loop of the PPC is implemented in python and interacts with the continuous model

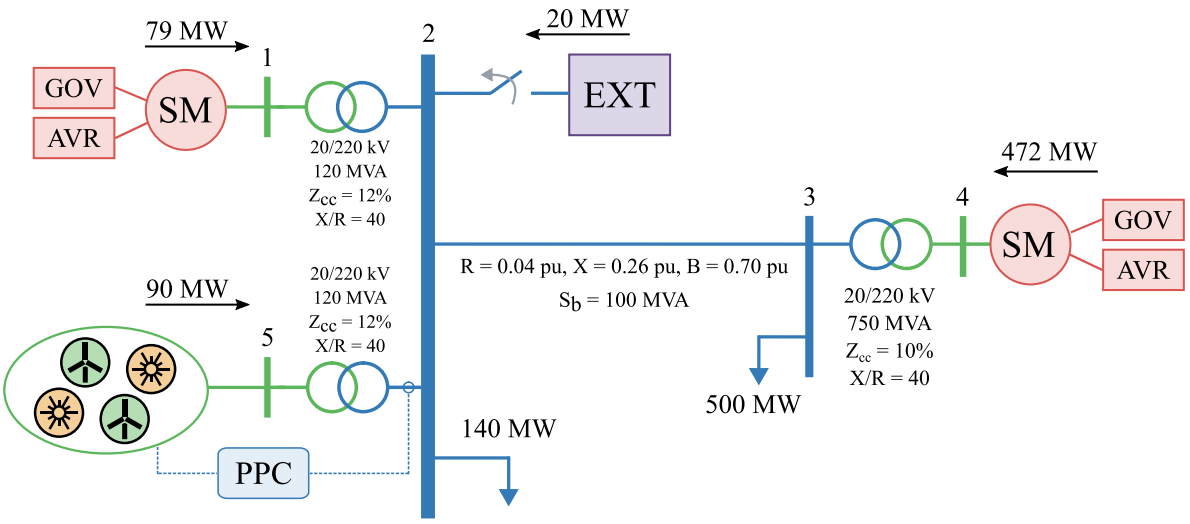

Fig. 4. Test system single-line diagram.

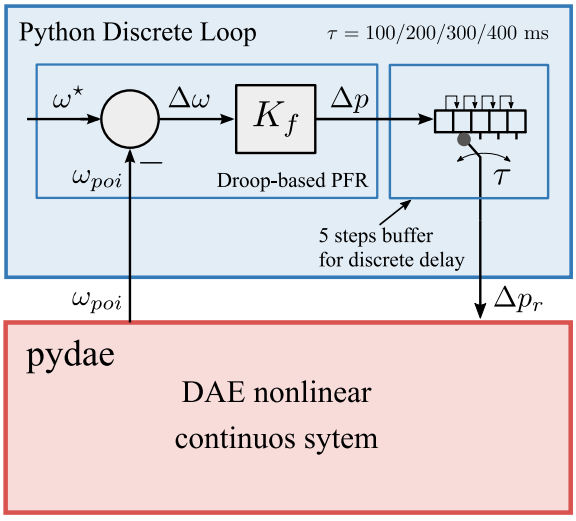

Fig. 5. Model implementation in pydae and Python.

of pydae to take frequency measurements and send active power set-points (see Fig. 5). The configured droop for the PPM PFR is 3% ($Droop = 1/K_f = \Delta f/\Delta P$), a value within the typical range specified in GCCs (e.g. 2%–12% for the European case [7]). Both types of considered delays, SSD and TD, are analysed and simulated.

The system is disturbed by an unbalance among power generation and consumption, leading to an under-frequency event that impacts the less damped oscillations modes of the system. This disturbance can be caused by the loss of a power generation plant, the disconnection of a line or a change in power consumption. In this case, the disturbance was simulated by opening a line, which resulted in a reduction of 20 MW of imported active power, approximately 3% of power consumption. (see Fig. 4, line between bus 2 and EXT). The objective of this dynamic study is to analyse the PFR of the PPM and its impact on power oscillation modes of interest.

3.2. Simulations with SSD

In this section, the benchmark scenario defined above has been simulated considering delays modelled as SSD. The results obtained for different time delays are shown in Figs. 6 to 8. In particular, the following case studies are analysed: PPM without PFR response in black; and PPM with PFR response for 100 ms (in red), 200 ms (in green), 300 ms (in blue) and 400 ms (in yellow) time delays.

In Fig. 6 the system modes in the complex plane are represented establishing different areas for the different damping amplitudes. Fig. 7 represents the evolution of the Center Of Inertia (COI) frequency as well as the total active power contribution of the IBRs that conforms the PPM for different values of the communication delay between IBRs and the PPC.

The small signal analysis presented in Fig. 6 shows that with τ = 100 ms the critical mode is better damped than in the case in which there are not PFR. However, when τ = 200 ms the damping is significantly impacted, resulting in it falling below an intolerable threshold of less than 5%. The same results are obtained for a τ = 300 ms that is again improved for a value of τ = 400 ms. Table 2 complements these findings by providing the numerical values of the critical oscillation mode for each case study, including the real part, imaginary part, frequency, and damping ratio. As it can be seen, the PPM performing PFR has a high impact on the least damped electromechanical mode, mainly associated with the synchronous machine at bus 1, where ω_1 and δ_1 are the state variables with the highest participation. In sight of these results, it can be concluded that increasing the plant response time can improve or worsen the damping of the system, being necessary to perform a previous analysis of these possible delays to avoid compromising the dynamic stability of the power system. Focusing on the time-domain response presented in Fig. 7, the results confirm the behaviour predicted by the small-signal analysis. The frequency without PFR is shown in black, displaying the greatest nadir. The addition of PFR decreases the maximum deviation, as expected, improving when the PPC control latency taken into account is smaller. To observe the predicted decrease in oscillation damping, the speed difference between the synchronous generators at buses 1 and 4 has been calculated and plotted in Fig. 8 for all simulated cases. A zoom at the bottom of the plot clearly indicates that a value of Δt = 300 ms results in the worst damping.

Additional small signal analysis results have been included to demonstrate that the damping of system oscillation modes depends not only on PFR delays, but also on factors such as tie-line length (see Fig. 9) and system inertia distribution (see Fig. 10). These results consider an SSD delay of 400 ms, one of the cases where the critical mode exhibits a damping greater than 5% in the comparison shown in Fig. 6. In this configuration, the critical mode of the system moves into the poorly damped region (represented in red) as the tie-line length increases and the inertia of SM at bus 4 decreases.

Table 2
Summary of critical oscillation mode for different discretization times (SSD model).

Case study	Re (1/s)	Im (rad/s)	Freq (Hz)	Damping (%)
no PFR	−0.46	7.13	1.13	6.41
100 ms	−0.57	7.35	1.17	7.77
200 ms	−0.30	7.31	1.16	4.04
300 ms	−0.26	7.08	1.13	3.65
400 ms	−0.40	6.97	1.11	5.76

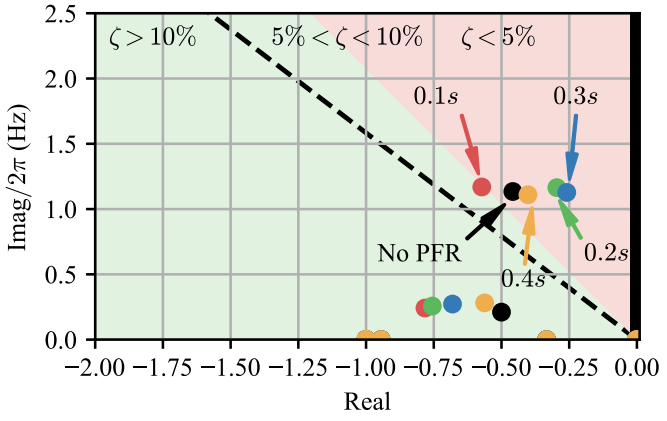

Fig. 6. Root locus for different discretization times (SSD model).

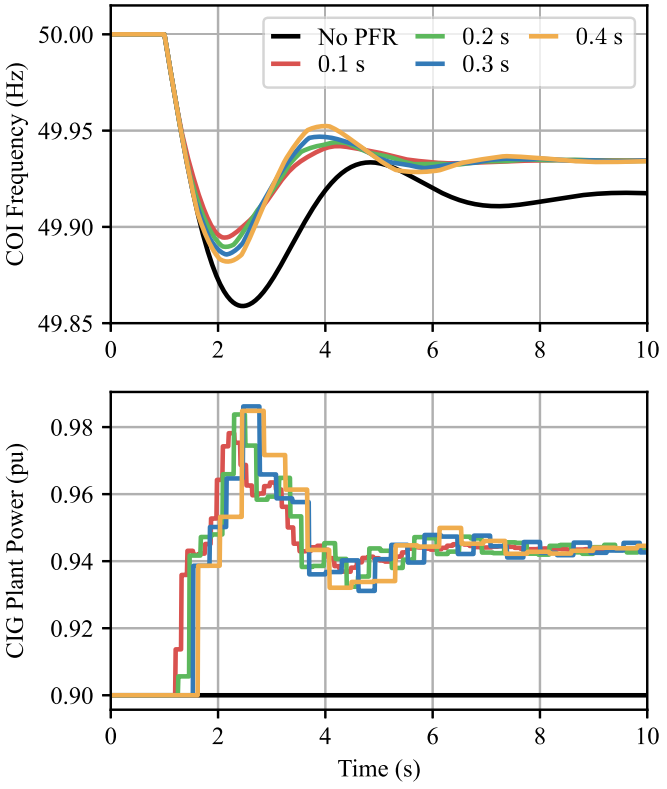

Fig. 7. Frequency variation and PPM PFR (SSD model).

3.3. Simulations with TD

Similar issues arise when transport delays are considered. Fig. 11 shows the location of the system modes for the different time delay amplitudes, complemented by the numerical values of the critical mode

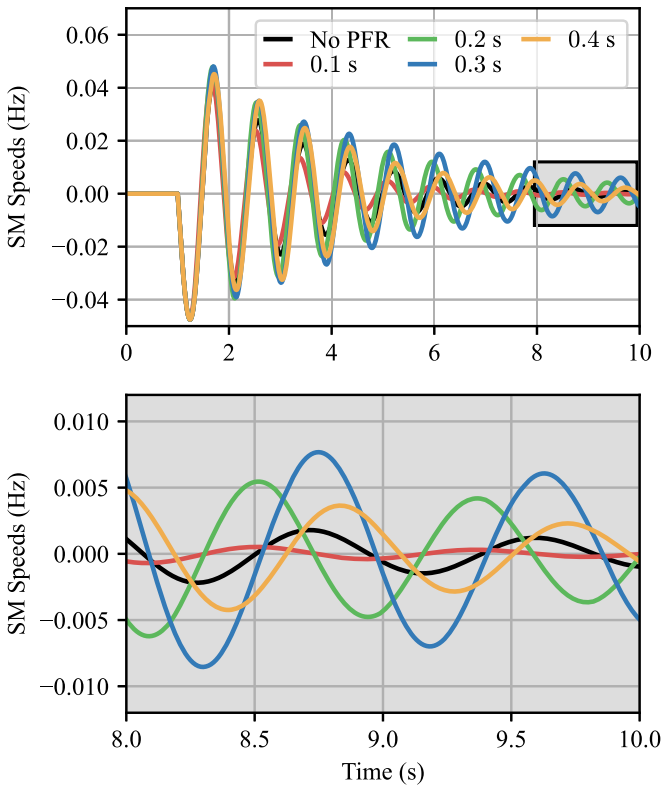

Fig. 8. Relative speeds between both synchronous machines (SSD model).

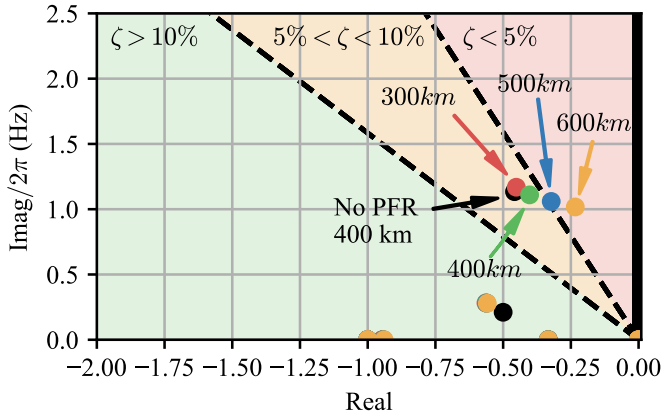

Fig. 9. Root locus for different lengths of line 2–3 and discretization time of 0.4 s (SSD model).

presented in Table 3. Fig. 12 presents the results of a time-domain simulation, depicting the evolution of the frequency variations and the active power contributions of the IBRs. Finally, Fig. 13 shows the speed difference between the synchronous generators at buses 1 and 4.

In this case, the damping deteriorates as the considered delay increases, with the exception of 1τ, case for which the damping of the system improves even with respect to the no-PFR provision by the PPM. Again, Fig. 12 shows how the nadir decreases as the communication delay decreases. However, as observed in the analysis of the system modes, this fact does not coincide with an improvement in the system damping. Fig. 13 shows that for a delay of 4τ, the oscillations between the two synchronous machines within low frequencies reach their maximum in amplitude.

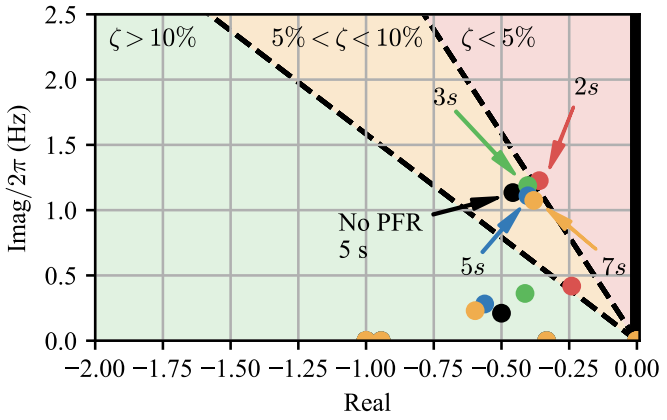

Fig. 10. Root locus for different inertia of Bus 4 SM and discretization time of 0.4 s (SSD model).

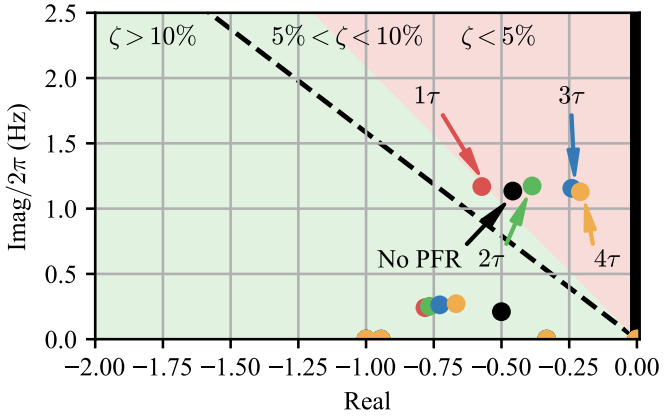

Fig. 11. Root locus for different delays (TD model).

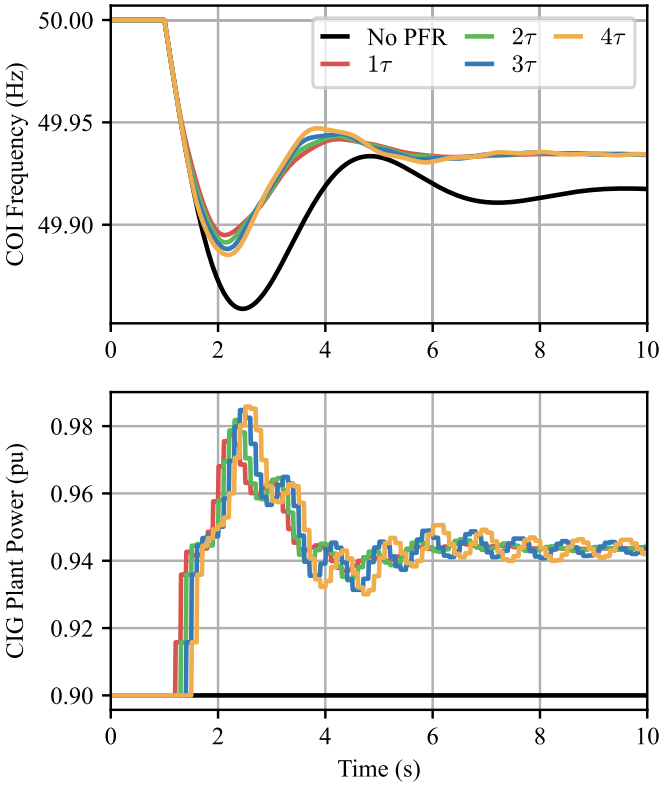

Fig. 12. Frequency variation and PPM PFR (TD model).

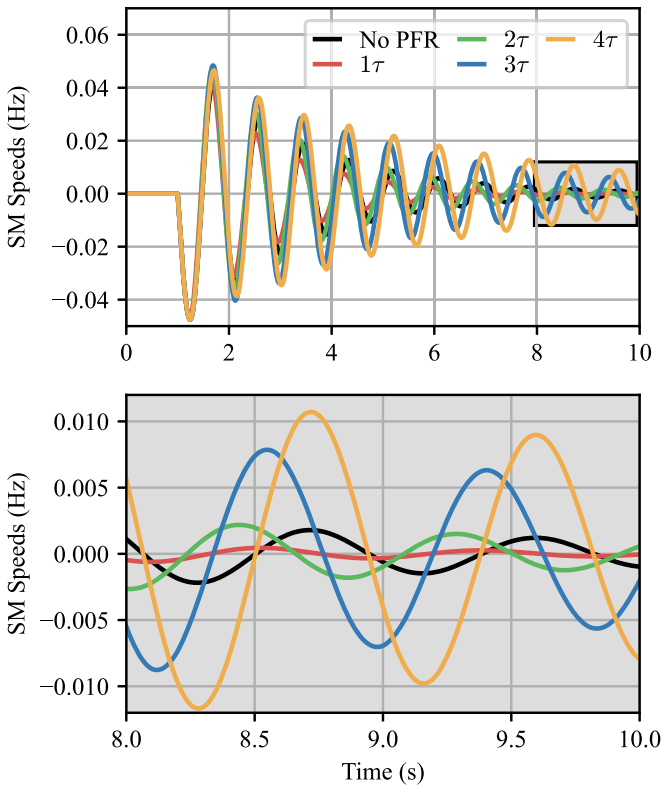

Fig. 13. Relative speeds between both synchronous machines (TD model).

Table 3
Summary of critical oscillation for different delays (TD model).

Case study	Re (1/s)	Im (rad/s)	Freq (Hz)	Damping (%)
no PFR	−0.46	7.13	1.13	6.41
100 ms	−0.57	7.35	1.17	7.77
200 ms	−0.39	7.38	1.17	5.24
300 ms	−0.24	7.26	1.16	3.31
400 ms	−0.21	7.09	1.13	2.95

4. Conclusions

With the expansion of renewable energy technologies and their converter-interfaced nature, the displacement of synchronous machines, along with the reduction of inertia and primary frequency response, has become a major concern. A commonly applied solution is to create extensive photovoltaic plants and wind farms that must provide PFR at the POI. Unlike synchronous machines, which perform this task locally at each generator, these renewable power plants require communication between the PPC and each individual generator. These communication delays affect the provision of PFR at the POI, which can deteriorate the damping of power oscillations within the power system to which they are connected.

This work has demonstrated the degradation that the damping of a power system can suffer when it is affected by typical delays in the communication between the PPC that governs a renewable power plant and the different generators that compose it. For this purpose, an analysis has been carried out using a detailed model of a two-area power system with a PPM performing PFR with different discrete delays (either in amplitude or in model). The results show that these delays cause a deterioration in the damping of low frequency oscillations in the face of frequency events. In addition, in the case of the SSD, which is the most common for centralized controllers, a longer delay does not necessarily result in lower damping.

The results highlight the critical importance of considering communication delays in the design and tuning of the PFR of Power Park Modules. Ignoring these delays can lead to degraded dynamic performance and even instability in low-inertia systems. These findings also serve as a foundation for exploring mitigation strategies, such as the implementation of feedforward compensators, adaptive control techniques, or the redesign of the PPC-inverter communication architecture to enhance responsiveness and robustness.

CRediT authorship contribution statement

Luna Moreno-Díaz: Writing – original draft, Software, Investigation, Data curation, Conceptualization. **Juan Manuel Mauricio:** Writing – review & editing, Software, Methodology, Funding acquisition. **Álvaro Rodríguez del Nozal:** Writing – review & editing, Supervision. **Jelena Stojkovic Terzic:** Writing – review & editing, Supervision.

Declaration of competing interest

The authors declare that they have no known competing financial interests or personal relationships that could have appeared to influence the work reported in this paper.

Acknowledgements

This work was partially supported by the Ministerio de Ciencia e Innovación (MCIN) Agencia Estatal de Investigación (AEI) 10.13039/501100011033 through the "European Regional Development Fund (ERDF) A way of making Europe" under Grant PID2021-127835OB-I00; and by the European Comission by the projects COCOON and SUNRISE under grant agreements 101120221 and 101079200, respectively.

Data availability

Data will be made available on request.

References

[1] International Renewable Energy Agency, Renewable Energy Highlights, 11 July 2024, International Renewable Energy Agency (IRENA), 2024, Available at https://www.irena.org/-/media/Files/IRENA/Agency/Publication/2024/Jul/Renewable_energy_highlights_FINAL_July_2024.pdf.

[2] M.S. Alam, F.S. Al-Ismail, A. Salem, M.A. Abido, High-level penetration of renewable energy sources into grid utility: Challenges and solutions, IEEE Access 8 (2020) 190277–190299, http://dx.doi.org/10.1109/ACCESS.2020.3031481.

[3] J. Shair, H. Li, J. Hu, X. Xie, Power system stability issues, classifications and research prospects in the context of high-penetration of renewables and power electronics, Renew. Sustain. Energy Rev. 145 (2021) 111111, http://dx.doi.org/10.1016/j.rser.2021.111111.

[4] N. Hatziargyriou, J. Milanovic, C. Rahmann, V. Ajjarapu, C. Canizares, I. Erlich, D. Hill, I. Hiskens, I. Kamwa, B. Pal, P. Pourbeik, J. Sanchez-Gasca, A. Stankovic, T. Van Cutsem, V. Vittal, C. Vournas, Definition and classification of power system stability – revisited and extended, IEEE Trans. Power Syst. 36 (4) (2021) 3271–3281, http://dx.doi.org/10.1109/TPWRS.2020.3041774.

[5] H. Bevrani, H. Golpîra, A.R. Messina, N. Hatziargyriou, F. Milano, T. Ise, Power system frequency control: An updated review of current solutions and new challenges, Electr. Power Syst. Res. 194 (2021) http://dx.doi.org/10.1016/j.epsr.2021.107114.

[6] V. Gevorgian, Y. Zhang, E. Ela, Investigating the impacts of wind generation participation in interconnection frequency response, IEEE Trans. Sustain. Energy 6 (2015) 1004–1012, http://dx.doi.org/10.1109/TSTE.2014.2343836.

[7] Commission Regulation (EU) 2016/631 of 14 April 2016 establishing a network code on requirements for grid connection of generators (Text with EEA relevance), no. 112, 2016, pp. 1–68, Available at http://data.europa.eu/eli/reg/2016/631/oj.

[8] C.N. de Control de la Energía (CENACE), Manual regulatorio de requerimientos técnicos para la interconexión de centrales eléctricas al sistema eléctrico nacional, 2021, pp. 217–241.

[9] A.E.M.C. (AEMC), S5.2 conditions for connection of generators, 2018, Available at https://tinyurl.com/australianps.

[10] P.R.E.P.A. (PREPA), Appendix E. Minimum Technical Requirements (MTR), Available at https://energia.pr.gov/wp-content/uploads/sites/7/2024/02/03-RE-RFP_Appednix-H_MTRs.pdf.

[11] C.N. de la Energía (CNE) de Santiago de Chile, Norma técnica de seguridad y calidad de servicio, 2024, Available at https://www.cne.cl/wp-content/uploads/2024/10/NTSyCS-Octubre-24.pdf.

[12] National Energy Regulator of South Africa (NERSA), Grid connection code for renewable power plants (RPPs) connected to the electricity transmission system (TS) or the distribution system (DS) in South Africa, 2022, Available at https://www.sseg.org.za/wp-content/uploads/2014/07/SAGC-Requirements-for-Renewable-Power-Plants-Rev-3.1.pdf.

[13] M. para la Transición Ecológica y el reto Demográfico, Orden TED/749/2020, de 16 de julio, por la que se establecen los requisitos técnicos para la conexión a la red necesarios para la implementación de los códigos de red de conexión., 2020, Available at https://www.boe.es/eli/es/o/2020/07/16/ted749.

[14] M. de Energía Turismo y Agenda Digital, Resolución de 1 de febrero de 2018, de la Secretaría de Estado de Energía, por la que se aprueba el procedimiento de operación 12.2 "Instalaciones conectadas a la red de transporte y equipo generador: requisitos mínimos de diseño, equipamiento, funcionamiento, puesta en servicio y seguridad" de los sistemas eléctricos no peninsulares, 2018, pp. 27–31, Available at https://www.boe.es/diario_boe/txt.php?id=BOE-A-2018-2198.

[15] P. Pourbeik, J.J. Sanchez-Gasca, J. Senthil, J.D. Weber, P.S. Zadehkhost, Y. Kazachkov, S. Tacke, J. Wen, A. Ellis, Generic dynamic models for modeling wind power plants and other renewable technologies in large-scale power system studies, IEEE Trans. Energy Convers. 32 (2017) 1108–1116, http://dx.doi.org/10.1109/TEC.2016.2639050.

[16] L. Moreno-Díaz, J.M. Mauricio, Controladores de Potencia de Plantas (PPC), Spanish Ministry of Industry and Tourism, 2024, Available at https://www.mintur.gob.es/Publicaciones/Publicacionesperiodicas/EconomiaIndustrial/RevistaEconomiaIndustrial/431/14_MORENO_1.pdf.

[17] W. Zhou, C. Li, L. Yang, Z. Li, C. Zhang, T. Zheng, Analysis of primary frequency regulation characteristics of PV power plant considering communication delay, Energy Rep. 9 (2023) 1315–1325, http://dx.doi.org/10.1016/j.egyr.2023.04.176.

[18] F. Milano, F. Dörfler, G. Hug, D.J. Hill, G. Verbič, Foundations and challenges of low-inertia systems (invited paper), in: 2018 Power Systems Computation Conference, PSCC, 2018, pp. 1–25, http://dx.doi.org/10.23919/PSCC.2018.8450880.

[19] F. Milano, M. Anghel, Impact of time delays on power system stability, IEEE Trans. Circuits Syst. I. Regul. Pap. 59 (4) (2012) 889–900, http://dx.doi.org/10.1109/TCSI.2011.2169744.

[20] M.N.H. Shazon, N.-A. Masood, A. Jawad, Frequency control challenges and potential countermeasures in future low-inertia power systems: A review, Energy Rep. 8 (2022) 6191–6219, http://dx.doi.org/10.1016/j.egyr.2022.04.063.

[21] Y. Zhang, N. Wiese, Z. Liu, M. Braun, On the control interaction of synchronous machine and inverter-based resources during system-split situations, Int. J. Electr. Power Energy Syst. 152 (2023) 109227, http://dx.doi.org/10.1016/J.IJEPES.2023.109227.

[22] A. Kannan, M. Nuschke, B.P. Dobrin, D. Strauß-Mincu, Frequency stability analysis for inverter dominated grids during system split, Electr. Power Syst. Res. 188 (2020) http://dx.doi.org/10.1016/j.epsr.2020.106550.

[23] M. Nuschke, B.O. Winter, D. Strauß-Mincu, B. Engel, Power System Stability Analysis for System-Split Situations with Increasing Shares of Inverter Based Generation, in: NEIS Conference 2019, 2019.

[24] F. Milano, Power System Modelling and Scripting, in: Power Systems, Springer Berlin Heidelberg, 2010, URL https://books.google.es/books?id=MQu7IqoLrfYC.

[25] N. Jankovic, J. Roldán-Pérez, M. Prodanovic, L. Rouco, Centralised multimode power oscillation damping controller for photovoltaic plants with communication delay compensation, IEEE Trans. Energy Convers. 39 (1) (2024) 311–321, http://dx.doi.org/10.1109/TEC.2023.3317577.

[26] L. Moreno, D. Señas, D. Fernández, J. González, E. Hayas, F. Holik, I. Corleoni, G. Kryonidis, F. Fotellis, A. Marnerides, D8.1 secure DRES deployments pilot design and configuration. COCOON project funded by horizon europe (HORIZON-CL3-2022-CS-01), 2025.

[27] F. Wilches-Bernal, B.J. Pierre, R.T. Elliott, D.A. Schoenwald, R.H. Byrne, J.C. Neely, D.J. Trudnowski, Time delay definitions and characterization in the pacific DC intertie wide area damping controller, in: IEEE Power Energy Society General Meeting, 2017, pp. 1–5, http://dx.doi.org/10.1109/PESGM.2017.8274082.

[28] J.M. Mauricio, A.E. Leon, Improving small-signal stability of power systems with significant converter-interfaced generation, IEEE Trans. Power Syst. 35 (4) (2020) 2904–2914, http://dx.doi.org/10.1109/TPWRS.2020.2968422.

[29] P. Kundur, N. Balu, M. Lauby, Power System Stability and Control, in: EPRI Power System Engineering Series, McGraw-Hill, 1994, URL https://tinyurl.com/kundurbook.

[30] J.M. Mauricio, Pydae library website, 2023, Available at https://pydae-bmapu.readthedocs.io/.